

**Gas density and X-ray surface brightness profiles
of clusters of galaxies from dark matter halo potentials:
beyond the isothermal β model**

Yasushi Suto^{1,2}, Shin Sasaki³, and Nobuyoshi Makino^{4,5}

¹ Department of Physics, University of Tokyo, Tokyo 113-0033, Japan

² Research Center for the Early Universe (RESCEU), School of Science
University of Tokyo, Tokyo 113-0033, Japan

³ Department of Physics, Tokyo Metropolitan University, Hachioji, Tokyo 192-0397, Japan

⁴ Department of Physics, Ritsumeikan University, Kusatsu, Shiga, 525-8577, Japan

⁵ present address: Department of Mechanical Engineering
Oita National College of Technology, 1666 Maki, Oita 870-0152, Japan

e-mail: suto@phys.s.u-tokyo.ac.jp, sasaki@phys.metro-u.ac.jp, makino@oita-ct.ac.jp

ABSTRACT

We describe a theoretical framework to compute the cluster gas distribution in hydrostatic equilibrium embedded in a class of spherical dark matter halo potentials. Unlike the conventional isothermal β -model, the present method provides a physical basis to directly probe the shape of dark matter halo from the observed X-ray surface brightness and temperature profiles of clusters of galaxies. Specifically, we examine the extent to which the resulting gas density and X-ray surface brightness profiles are sensitive to the inner slope of the dark matter halo density and other more realistic effects including the self-gravity of the gas and the polytropic equation of state. We also discuss a practical strategy to apply the present methodology to the actual cluster profiles from future X-ray observations.

Subject headings: cosmology: theory – dark matter – galaxies: clusters: general – X-rays: galaxies

Accepted for publication in The Astrophysical Journal

1. Introduction

The gas density profiles of X-ray clusters of galaxies are known to be approximated well by the empirical formula, the isothermal β -model:

$$n_g(r) = \frac{n_{g0}}{[1 + (r/r_c)^2]^{3\beta/2}}. \quad (1)$$

Theoretically this is consistent with the observed indication that luminous member galaxies obey the King profile and the assumption of the hydrostatic equilibrium of cluster gas. The galaxies in clusters, however, constitute a very small fraction of the gravitational mass of the entire cluster due to the presence of dark matter. Recent high-resolution N-body/hydrodynamical simulations have strongly suggested that dark halos of cluster scales are described by a family of fairly universal density profiles. Navarro, Frenk & White (1996,1997, hereafter NFW) proposed a profile:

$$\rho_{\text{DM}}(r) = \frac{\delta_c \rho_{c0}}{(r/r_s)(1 + r/r_s)^2}, \quad (2)$$

where ρ_{c0} is the critical density of the universe at $z = 0$, and δ_c and r_s are the concentration parameter and the scaled radius whose explicit fitting formulae as a function of the halo mass M and cosmological parameters are found in Navarro, Frenk & White (1997).

This enables one to predict the profiles of the gas and the X-ray surface brightness. Our previous work (Makino, Sasaki & Suto 1998, hereafter Paper I) examined the case of the NFW profile proposed, and found that the resulting gas density profile is very close to the empirical model (1).

Higher-resolution N-body simulations by Fukushige & Makino (1997), however, indicate that the inner density profile of the halo is much steeper than the NFW profile above. This conclusion was confirmed later by a series of systematic N-body simulations by Moore et al. (1998). Evans & Collett (1997) show that under some constraints the density profile $\propto r^{-4/3}$ becomes the stationary solution to the collisionless Boltzmann equation. Furthermore, in Paper I we assumed the isothermality and the possible effect of the temperature profile was neglected. The present paper explores these effects in more details and provides several useful working formulae for the X-ray surface brightness profiles as well. In what follows we describe various theoretical formulation and do not attempt to compare with real observational data. The comparison with observations in this context has been performed by Makino & Asano (1998), Tamura (1998), Xu et al. (1998) and Markevitch et al. (1998). While all of their results indicate that the current observational data are consistent with the predictions in the universal density profile, the current data quality in the spatial resolution of X-ray surface brightness and temperature profiles is not sufficient in distinguishing from the empirical β -model in an unambiguous manner. In this respect, upcoming X-ray missions including AXAF and XMM should definitely provide us the data suitable for that purpose. This is mainly why we do not attempt any tentative comparison with the currently available data, but rather present various theoretical predictions which will be useful for future data analysis.

The plan of the paper is as follows; in §2 we describe a new series of analytical solutions for a family of density profiles of dark matter halos generalizing Paper I. Then we examine effects of self-gravity of the gas in §3, and non-isothermality by adopting polytropic equation of state in §4. Finally §5 is devoted to discussion and conclusions.

2. Isothermal gas and X-ray surface brightness profiles from a family of dark matter halo potentials

We generalize the NFW profile (2), and consider a family of density profiles describing the dark matter halo:

$$\rho_{\text{DM}}(x) = \frac{\delta_c \rho_{c0}}{x^\mu (1 + x^\nu)^\lambda}, \quad (3)$$

where $x \equiv r/r_s$ is the dimensionless radius in units of the characteristic scale r_s . Then the total mass of dark matter halo within the radius r is given by

$$M(r) = 4\pi \delta_c \rho_{c0} r_s^3 m(r/r_s), \quad (4)$$

with

$$m(x) \equiv \int_0^x \frac{u^{2-\mu}}{(1 + u^\nu)^\lambda} du. \quad (5)$$

If one neglects the gas and galaxy contributions to the gravitational mass, the gas density profile $\rho_g(r)$ in hydrostatic equilibrium with the above dark matter potential satisfies

$$\frac{kT_g}{\mu_g m_p} \frac{d \ln \rho_g}{dr} = -\frac{GM(r)}{r^2}, \quad (6)$$

where μ_g and m_p denote the mean molecular weight of the gas (we adopt 0.59 below) and the proton mass, and we assume that the gas temperature T_g is constant over the cluster (non-isothermal cases are considered in §4). Equation (6) can be formally integrated to yield

$$\ln \frac{\rho_g(r)}{\rho_{g0}} = -B \int_0^{r/r_s} \frac{m(x)}{x^2} dx, \quad (7)$$

where

$$B \equiv \frac{4\pi G \mu_g m_p \delta_c \rho_{c0} r_s^2}{kT_g}. \quad (8)$$

Note that B is $27b/2$ in terms of the parameter b defined in Paper I. Also B is rewritten as

$$B = \frac{3}{\gamma m(1)} \frac{T_{\text{vir}}(r_s)}{T_g} \quad (9)$$

in terms of the virial temperature defined as

$$T_{\text{vir}}(r) \equiv \gamma \frac{G \mu_g m_p M(r)}{3kr} \quad (10)$$

with $\gamma(\approx 1 - 2)$ being a fudge factor (see Paper I).

With the density profile of the form (3), equation (7) converges for $\mu < 2$, and is rewritten as

$$\rho_g(r) = \rho_{g0} \exp[-Bf(r/r_s)], \quad (11)$$

where

$$f(x) \equiv \int_0^x \frac{m(u)}{u^2} du = \int_0^x \frac{u^{1-\mu}}{(1+u^\nu)^\lambda} du - \frac{1}{x} \int_0^x \frac{u^{2-\mu}}{(1+u^\nu)^\lambda} du. \quad (12)$$

In some specific cases, equations (5) and (12) are analytically integrated:

(i) $\mu = 1, \nu = 1, \lambda = 2$ (NFW)

$$m(x) = \ln(1+x) - \frac{x}{1+x}, \quad (13)$$

$$f(x) = 1 - \frac{1}{x} \ln(1+x). \quad (14)$$

(ii) $\mu = 3/2, \nu = 3/2, \lambda = 1$

$$m(x) = \frac{2}{3} \ln(1+x^{2/3}), \quad (15)$$

$$f(x) = \frac{x-2}{3x} \ln(1+\sqrt{x^3}) + \ln(1+\sqrt{x}) + \frac{2}{\sqrt{3}} \tan^{-1} \frac{2\sqrt{x}-1}{\sqrt{3}} + \frac{\sqrt{3}}{9} \pi. \quad (16)$$

(iii) $\mu = 3/2, \nu = 1, \lambda = 3/2$

$$m(x) = 2 \ln(\sqrt{x} + \sqrt{1+x}) - 2\sqrt{\frac{x}{1+x}}, \quad (17)$$

$$f(x) = 2\sqrt{\frac{1+x}{x}} - \frac{2}{x} \ln(\sqrt{x} + \sqrt{1+x}). \quad (18)$$

In what follows, we focus on the case with $\mu = \alpha, \nu = 1, \lambda = 3 - \alpha$ ($1 < \alpha < 2$). Then equation (12) reduces to

$$f(x) = \int_0^x \frac{u^{1-\alpha}}{(1+u)^{3-\alpha}} du - \frac{1}{x} \int_0^x \frac{u^{2-\alpha}}{(1+u)^{3-\alpha}} du. \quad (19)$$

If we set $\alpha = 1$, equation (19) reduces to the case (i) which corresponds to the original proposal by Navarro, Frenk & White (1996,1997) and is worked out in Paper I. Since the power-law slope of the inner region is very sensitive to the mass resolution limit of numerical simulations (Fukushige & Makino 1997; Moore et al. 1998; Melott et al. 1997; Splinter et al. 1998), we explore the similar profiles by changing α . Since it is unlikely that the mass resolution limit affects the asymptotic outer halo profile $\propto r^{-3}$, we choose $\lambda = 3 - \alpha$ so as to reproduce the asymptotic behavior.

2.1. gas density profile

For $1 \leq \alpha \leq 2$, we numerically integrate equation (19) to compute the gas density profile which is proportional to $[F(x)]^B$ where we define

$$F(x) \equiv \exp[-f(x)]. \quad (20)$$

Figure 1 plots the $F(x)$ for $\alpha = 1.0, 1.4$ and 1.6 together with the empirical fit to the following function:

$$F_{\text{fit}}(x) = \left[1 + \left(\frac{x}{x_c(\alpha)} \right)^{q(\alpha)} \right]^{p(\alpha)}. \quad (21)$$

For $x \ll 1$, equations (19) to (21) are consistent if

$$q(\alpha) = 2 - \alpha \quad (22)$$

and

$$x_c^{2-\alpha} = (3 - \alpha)(2 - \alpha)p. \quad (23)$$

We adopt the relation (22), but still keep p and x_c as two independent parameters to fit the $F(x)$ in the range of $0.05 \leq x \leq 5$. The results are plotted in solid lines in Figure 1. For $1 < \alpha < 1.8$, we find the following empirical fitting formulae:

$$x_c(\alpha) = 0.015(2 - \alpha)^{-2.5} + 0.47(2 - \alpha)^{0.5}, \quad p(\alpha) = 0.33(2 - \alpha)^{-1.75}, \quad (24)$$

as plotted in Figure 2.

2.2. X-ray surface brightness profile

From the observational point of view, it is more useful to compute the X-ray surface brightness profile on the sky:

$$\Sigma_X(\theta) \equiv \frac{1}{(1+z)^4} \int_{-\infty}^{\infty} \alpha_X(T_g) n_e^2(\sqrt{\theta^2 d_A^2(z) + l^2}) dl, \quad (25)$$

where z is the redshift of the cluster considered, α_X is the X-ray (either bolometric or band-limited) emissivity, $n_e(r)$ is the electron number density corresponding to the profile (11), $d_A(z)$ is the angular diameter distance, and the integration is performed over the line-of-sight at an angular separation θ from the center of the cluster.

Substituting the isothermal density profiles (19) and (20), equation (25) reduces to

$$\Sigma_X(\theta) = \frac{2\alpha_X(T_g)n_{e0}^2 r_s}{(1+z)^4} S(\theta/\theta_s), \quad (26)$$

where $\theta_s \equiv r_s/d_A(z)$, and

$$S(\phi) \equiv \int_{\phi}^{\infty} \frac{x \exp[-2Bf(x)]}{\sqrt{x^2 - \phi^2}} dx. \quad (27)$$

Throughout the present paper we consider the X-ray bolometric emissivity, and truncate the gas density at $r = 20r_s$, i.e., $n_g(r) = 0$ at $r > 20r_s$ in evaluating the surface brightness to avoid unphysical divergence. This is because $20r_s$ is typically larger than the virial radius and the gas profile should not be extended at the larger scale. We integrate equation (27) numerically for $(\alpha, B) = (1.0, 5.0)$, $(1.0, 10.0)$, $(1.6, 10.0)$, and $(1.6, 20.0)$, and the results are plotted in Figure 3. They cannot be reasonably fitted to the conventional β -model:

$$S(\phi) = \frac{S(0)}{[1 + (\phi/\phi_{c,\beta})^2]^{3\beta-1/2}}, \quad (28)$$

where β is the slope parameter, $\phi_{c,\beta}$ is the core radius, and $S(0)$ is the central surface brightness. Due to the strong concentration of the dark matter halo in the present models, the resulting gas density profiles are also more concentrated than the conventional β -model. In fact, the deviation from the β -model becomes more appreciable for a larger α . Rather we find that the following generalized shape:

$$S(\phi) \propto \frac{1}{[1 + (\phi/\phi_c)^\xi]^\eta} \quad (29)$$

with

$$\phi_c = 0.3 \left(\frac{2}{\alpha} - 1 \right), \quad (30)$$

$$\xi = 0.41 - 5.4(2 - \alpha)^6 + (0.585 + 6.47\alpha^{-5.18})B^{-\alpha^6/30}, \quad (31)$$

$$\eta = -0.68 - 5.09(\alpha - 1)^2 + (0.202 + 0.0206\alpha^8)B^{1.1}, \quad (32)$$

provides an excellent fit for $5 \leq B \leq 20$ and $1.0 \leq \alpha \leq 1.6$ in the range of $10^{-4} \leq \phi \leq \phi_{\max}$ where $S(\phi_{\max}) = 10^{-4}S(0)$.

Provided that the assumption of the isothermal gas is valid for actual clusters, our fitting formulae above can be used directly to probe the shape of the dark matter halo; fitting the observed X-ray surface brightness to equations (29) to (32) would result in the values of α , r_s and B from the three fitted parameters $\theta_s\phi_c$, ξ and η . In addition if the gas temperature T_g is measured from X-ray spectroscopic observations, the concentration parameter δ_c is determined via equation (8).

Incidentally let us note that our fitting formulae (29) are not unique in the sense that the three parameters ϕ_c , ξ and η are correlated and written in terms of the two independent parameters α and B . In particular, ϕ_c and ξ are strongly correlated, and we would obtain an equally good fitting formula by changing these two appropriately. On the other hand, η is relatively insensitive to the choice of ϕ_c or ξ .

Applying the procedure described above to three lensing clusters (A2163, A2218 and RX J1347.5-1145), Makino & Asano (1998) showed that the dark matter profile with $\alpha \leq 1.4$ is consistent with the *ROSAT* HRI X-ray surface brightness profiles, and that $\alpha \sim 1.4$ is preferred in order for the X-ray mass estimate to be consistent with their giant arcs. Tamura (1998) also reached the similar conclusion on the basis of ASCA/*ROSAT* observation of A1060.

3. Effect of self-gravity of the gas density distribution

When one properly includes the self-gravity of the gas distribution, equation (6) reads

$$\frac{kT_g}{\mu_g m_p} \frac{d \ln \rho_g}{dr} = -\frac{GM_{\text{tot}}(r)}{r^2} = -\frac{4\pi G}{r^2} \int_0^r u^2 [\rho_{\text{DM}}(u) + \rho_g(u)] du. \quad (33)$$

With the profile (3) for dark matter halo, the above equation is rewritten in a non-dimensional form as

$$\frac{dg(x)}{dx} = -\frac{B}{x^2} \int_0^x \left[\frac{1}{u^\mu (1+u^\nu)^\lambda} + R e^{g(x)} \right] u^2 du, \quad (34)$$

where we introduce

$$g(x) \equiv \ln[\rho_g(x)/\rho_{g0}] \quad \text{and} \quad R \equiv \rho_{g0}/(\delta_c \rho_{c0}). \quad (35)$$

For $\mu = \alpha$, $\nu = 1$ and $\lambda = 3 - \alpha$, the lowest-order perturbation solution for equation (34) at $x \ll 1$ is

$$g(x) \approx -\frac{B}{(3-\alpha)(2-\alpha)} x^{2-\alpha}. \quad (36)$$

In Figure 4, we consider the effect for the NFW profile ($\alpha = 1$) only, and numerically integrate the second-order differential equation:

$$\frac{d^2 g(x)}{dx^2} + \frac{2}{x} \frac{dg(x)}{dx} + B \left[\frac{1}{x(1+x)^2} + R e^{g(x)} \right] = 0, \quad (37)$$

where we rewrite equation (34) with the boundary condition specified from equation (36). The range of R is chosen so that the resulting gas to dark halo ratio:

$$f_g(x) \equiv \frac{M_g(x)}{M_{\text{DM}}(x)} = \frac{R}{\ln(1+x) - x/(1+x)} \int_0^x e^{g(u)} u^2 du, \quad (38)$$

approximately ranges $10^{-3} \sim 10^{-1}$ at $x = 10$.

We plot the gas density profiles including the effect of self-gravity in Figure 4a. With increasing the gas fraction or R , the gas density profile becomes steeper at large radii where the self-gravity of gas becomes significant compared with that of dark matter and confines the gas itself more strongly. Also as B increases, the gas distribution becomes more centrally concentrated since the gas temperature T_g and therefore the pressure gradient against the gravity becomes smaller for larger B .

In Figure 4b we present the gas mass fraction ($= M_g/[M_g + M_{\text{DM}}]$) for various values of B and R . At $x \lesssim 1$, ρ_{DM} is proportional to r^{-1} while ρ_{gas} is approximately constant. So the gas fractions of clusters in the present models increase roughly in proportional to x in the inner region. For larger x , on the other hand, the behavior is sensitive to the values of B and R . The observed baryon fraction of $0.1 \sim 0.2$ of clusters indicate that $(B, R) = (10, 5)$ and $(5, 1)$ fall in an observationally relevant range. In this case, the effect of gas self-gravity is not significant, but

cannot be fully neglected either. Also note that the gas mass fraction does not level off anywhere. Since the gas mass fraction provides an important constraint on the density parameter Ω_0 (e.g., White et al. 1993), this indicates the need for the quantitative comparison on the basis of the numerical integration of the above equation. As discussed in §6, this methodology is feasible under the generalized halo potential model.

4. Example of non-isothermal distribution: polytropic equation of state

In the discussion above, we have assumed the isothermal gas distribution. Although this is regarded as a reasonable approximation to the actual clusters, it is true that some clusters do show non-isothermal features. In particular, Markevitch et al. (1997) reported that the temperature profiles of clusters appear remarkably similar, and are approximately described by a polytrope with the polytropic index $\Gamma = 1.2 - 1.3$ *assuming* that the gas density profile is given by the β -model. In this section, we consider the effect of non-isothermal gas distribution on the basis of the polytropic equation of state for definiteness. More specifically, we adopt the following form for the gas pressure P :

$$P = P_0(\rho_g/\rho_{g0})^{1+1/n}, \quad (39)$$

or equivalently for the gas temperature:

$$T_g = T_{g0}(\rho_g/\rho_{g0})^{1/n}, \quad (40)$$

where the subscript 0 denotes the value at the center ($x = 0$), and the polytropic index Γ is equal to $1 + 1/n$.

As before we assume that the gas is in hydrostatic equilibrium:

$$\frac{1}{\rho_g} \frac{dP}{dr} = -\frac{GM(r)}{r^2}, \quad (41)$$

and neglect the self-gravity of the gas density. Define the function $\epsilon(x)$:

$$\epsilon(x) \equiv [\rho_g(x)/\rho_{g0}]^{1/n} = T_g(x)/T_{g0}, \quad (42)$$

then equation (41) is written in a dimensionless form as

$$\frac{d\epsilon}{dx} = -B_p \frac{m(x)}{x^2}, \quad (43)$$

where the constant B_p is defined as

$$B_p \equiv \frac{4\pi G}{n+1} \frac{\mu_g m_p \rho_{c0} \delta_c r_s^2}{k T_{g0}} = \frac{B}{n+1}. \quad (44)$$

Note that as in equation (9) B_p is related to $T_{\text{vir}}(r_s)$ as

$$B_p = \frac{3}{(n+1)\gamma m(1)} \frac{T_{\text{vir}}(r_s)}{T_{g0}}. \quad (45)$$

Equation (43) is integrated using the function $f(x)$ (eq.[12]) to yield

$$\epsilon(x) = 1 - B_p f(x). \quad (46)$$

Throughout the rest of this section we consider the NFW profile only just for illustration, but the discussion below can be easily generalized to other profiles.

The temperature and gas profiles in the present polytropic model are determined by specifying the two parameters, B_p and n . It should be noted that the upper limit on B_p is set by the maximal extension of the cluster gas; if the gas extends up to $x = x_{\max}$, then

$$B_p < B_{p,\max} \equiv 1/f(x_{\max}). \quad (47)$$

In the case of the NFW profile, $B_{p,\max}$ are 1.32, 1.18 and 1 for $x_{\max} = 10, 20$ and ∞ , respectively. With equation (45), the above condition (47) can be translated to the lower limit on the central gas temperature as

$$T_{g0} > \frac{3T_{\text{vir}}(r_s)}{(n+1)\gamma B_{p,\max} m(1)} \sim \frac{15T_{\text{vir}}(r_s)}{(n+1)\gamma}. \quad (48)$$

The resulting temperature and gas profiles are plotted in Figure 5. Note that $T_g(x)/T_{g0}$ is determined by B_p and the halo shape parameters only and is independent of the value of n , while the resulting gas density profile is sensitive to n . The gas temperature in the present models starts to decrease appreciably around at $x \gtrsim 1$ (solid lines in Fig.5a), where the density profile departs significantly from that in the corresponding isothermal model (dashed lines in Fig.5b). The virial temperature of the halo $T_{\text{vir}}(x)$ is significantly different from the gas temperature $T_g(x)$ in the present models (also in the isothermal model) indicating the importance of the detailed numerical simulations (e.g., Eke, Cole & Frenk 1998; Bryan & Norman 1998; Yoshikawa, Itoh, & Suto 1998) in predicting the temperature profile of clusters even in the present context.

Figure 6 shows the mass profile and gas mass fraction for polytropic models in comparison with those for isothermal cases. The gravity of gas mass is neglected, and for definiteness we choose the gas mass to be 10 percent of that of the dark halo at $x = 10$ which roughly corresponds to the virial radius in the NFW model.

The X-ray surface brightness and the emission-weighted temperature profiles on the sky, $\Sigma_X(\theta)$ and $T_X(\theta)$, are defined by equation (25) and

$$T_X(\theta) \equiv \frac{\int_{-\infty}^{\infty} T_g \alpha_X(T_g) n_e^2 (\sqrt{\theta^2 d_A^2(z) + l^2}) dl}{\int_{-\infty}^{\infty} \alpha_X(T_g) n_e^2 (\sqrt{\theta^2 d_A^2(z) + l^2}) dl}, \quad (49)$$

respectively. If we consider the bolometric thermal bremsstrahlung emissivity only, the polytropic models which we described above yield

$$\frac{\Sigma_X(\phi)}{\Sigma_X(0)} = \frac{\int_{\phi}^{\infty} \frac{x [\epsilon(x)]^{2n+1/2}}{\sqrt{x^2 - \phi^2}} dx}{\int_0^{\infty} [\epsilon(x)]^{2n+1/2} dx}, \quad (50)$$

$$\frac{T_X(\phi)}{T_X(0)} = \frac{\int_{\phi}^{\infty} \frac{x [\epsilon(x)]^{2n+3/2}}{\sqrt{x^2 - \phi^2}} dx}{\int_{\phi}^{\infty} \frac{x [\epsilon(x)]^{2n+1/2}}{\sqrt{x^2 - \phi^2}} dx} \frac{\int_0^{\infty} [\epsilon(x)]^{2n+1/2} dx}{\int_0^{\infty} [\epsilon(x)]^{2n+3/2} dx}, \quad (51)$$

where $\phi = \theta/\theta_s$ (§2.2). These profiles are plotted in Figure 7. The dotted curves in the upper panel indicate the best-fit β -model to the surface brightness. It is somewhat surprising that the X-ray surface brightness profiles for some models, e.g., with $(B_p, n) = (1.0, 7.0)$, are well approximated by the β -model despite the fact that the cluster is far from isothermal. It should be also noted here that the projected emission-weighted temperature $T_X(\theta)$ systematically differs from the gas temperature $T_g(r)$ evaluated at $\theta = r/d_A$ (e.g., Figs.5a and 7b).

5. Discussion and conclusions

In this paper, we have presented a physical methodology to confront the dark matter halo mass distribution with the observed X-ray surface brightness profiles of the galaxy cluster. Unlike the previous phenomenological prescriptions including the isothermal β -model, this approach enables one to determine the dark matter halo profile directly from the observational data. This works in an especially straightforward manner when the cluster is well approximated as isothermal; then our fitting formulae (eqs.[24], [31] to [32]) explicitly links the gas density and X-ray surface brightness profiles to the underlying dark matter halo potential as long as the halo is described by a family of profiles (eq.[3]). In §4, we have described a prescription of computing the gas, temperature, and X-ray surface brightness profiles for clusters with polytropic equation of state. We confirm that the self-gravity of the gas does not affect the density profile significantly (§3) in the halo profiles considered throughout the paper. Incidentally Bardelli et al. (1996) claimed that the gas mass fraction in A3558 (Shapley 8) is ~ 0.7 at the Abell radius (assuming $H_0 = 50 \text{ km s}^{-1} \text{ Mpc}^{-1}$). If confirmed, the X-ray surface brightness profile for such clusters should be computed with properly taking account of the self-gravity of gas, which is in fact feasible as shown below.

When both the self-gravity of gas density and the polytropic equation of state are taken into account, our procedure described in the present paper is generalized as follows;

- (i) select a dark matter halo density profile parameterized by (μ, ν, λ) :

$$\rho_{\text{DM}}(r) = \frac{\delta_c \rho_{c0}}{x^\mu (1 + x^\nu)^\lambda}. \quad (52)$$

- (ii) fix B_p (eq.[44]), R (eq.[35]) and the polytropic exponent n .

- (iii) solve the following equation for $\epsilon(x)$

$$\frac{d^2 \epsilon}{dx^2} + \frac{2}{x} \frac{d\epsilon}{dx} + B_p \left[\frac{1}{x^\mu (1 + x^\nu)^\lambda} + R \epsilon^n \right] = 0, \quad (53)$$

with the boundary condition at $x \ll 1$:

$$\epsilon(x) = 1 - \frac{B_p}{(2 - \mu)(3 - \mu)} x^{2-\mu}. \quad (54)$$

(iv) then one obtains $T_g(x) = T_{g0} \epsilon(x)$ and $\rho_g(x) = \rho_{g0} [\epsilon(x)]^n$, and finally can compute the corresponding X-ray surface brightness $\Sigma_X(\theta)$ which should be compared with an appropriate sample of X-ray clusters.

(v) repeat the above procedure to determine the set of parameters μ , ν , λ , n , B_p , and R . The latter two quantities are combined to yield the amplitude of the halo density $\delta_c \rho_{c0}$.

With the current and future spatially resolved X-ray surface brightness and temperature profiles of several clusters of galaxies with Einstein, ROSAT, ASCA, AXAF, and XMM, the present methodology will be a useful tool in revealing the shape of the underlying dark matter halo potential which one has not been able to derive, and thus provide important information on theories of cosmic structure formation.

We thank the editor, E.L. Wright, for detailed and invaluable comments on the earlier manuscript. This research was supported in part by the Grants-in-Aid for the Center-of-Excellence (COE) Research of the Ministry of Education, Science, Sports and Culture of Japan (07CE2002) to RESCEU (Research Center for the Early Universe), University of Tokyo, Japan.

REFERENCES

- Bardelli, S., Zucca, E., Malizia, A., Zamorani, G., Scaramella, R., & Vettolani, G. 1996, *A&A*, 305, 435
- Bryan, G.L. & Norman, M.L. 1998, *ApJ*, 495, 80
- Evans, N.W. & Collett, J.L. 1997, *ApJ*, 480, L103
- Fukushige, T., & Makino, J. 1997, *ApJ*, 477, L9
- Ikebe et al. 1997, *ApJ*, 481, 660
- Makino, N. & Asano, K. 1998, submitted to *ApJ*.
- Makino, N., Sasaki, S., & Suto, Y. 1998, *ApJ*, 497, 555 (Paper I)
- Markevitch, M., Forman, W.R., Sarazin, C.L., & Vikhlinin, A. 1998, *ApJ*, in press (astro-ph/9711289).
- Moore, B., Governato, F., Quinn, T., Stadel, J., & Lake, G. 1998, *ApJ*, 499, L5
- Navarro, J.F., Frenk, C.S., & White, S.D.M. 1996, *ApJ*, 462, 563
- Navarro, J.F., Frenk, C.S., & White, S.D.M. 1997, *ApJ*, 490, 493
- Melott, A.L., Splinter, R.J., Shandarin, S.F., & Suto, Y. 1997, *ApJ*, 479, L79
- Splinter, R.J., Melott, A.L., Shandarin, S.F., & Suto, Y. 1998, *ApJ*, 497, 38
- Tamura, T. 1998, ph.D thesis (University of Tokyo), unpublished.
- White, S.D.M., Navarro, J.F., Evrard, A.E., & Frenk, C.S. 1993, *Nature*, 366, 429
- Xu, H., Makishima, K., Fukazawa, Y., Ikebe, Y., Kikuchi, K., Ohasi, T., & Tamura, T. 1998, *ApJ*, 500, 738
- Yoshikawa, K., Itoh, M. & Suto, Y. 1998, *PASJ*, 50, 203

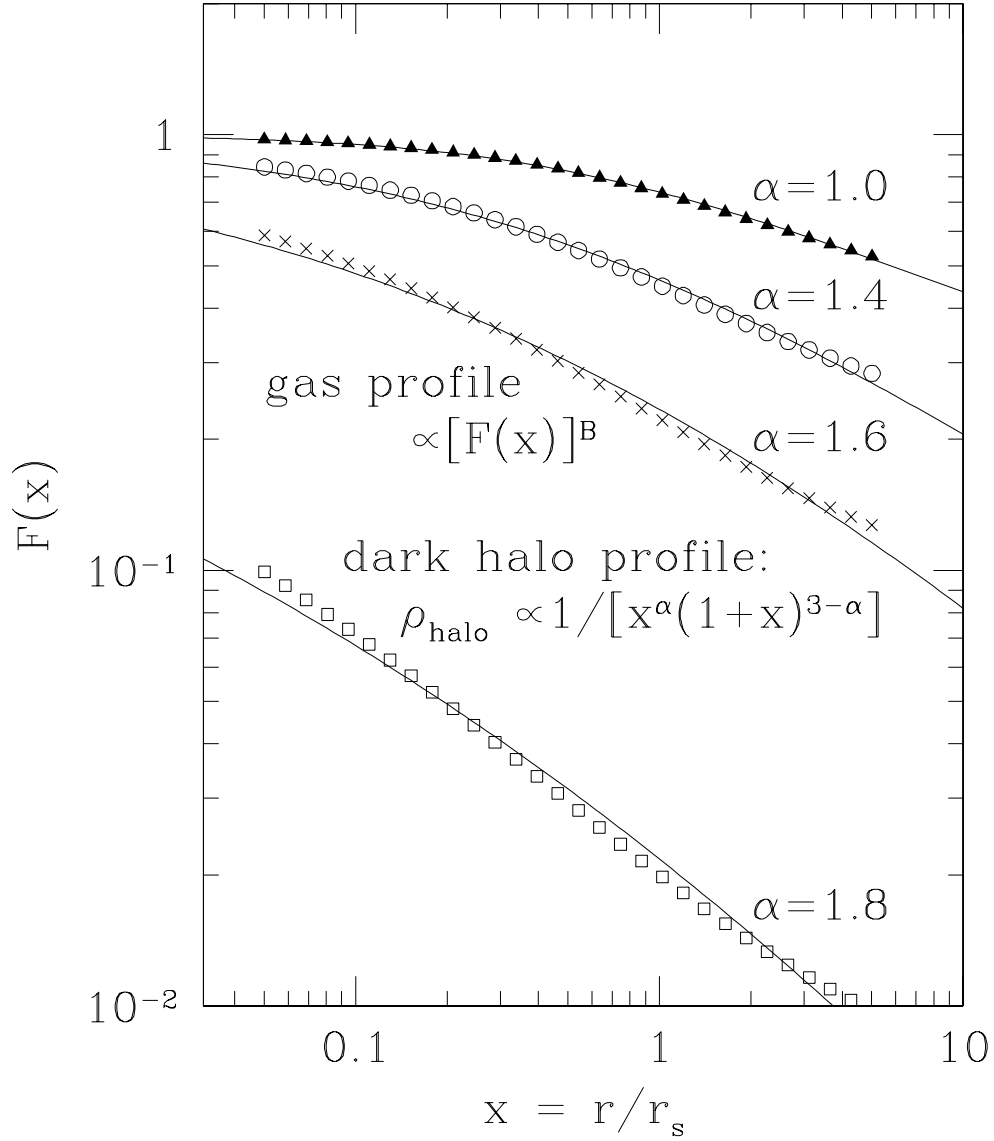


Fig. 1.— Gas density profiles predicted from a family of dark matter halo profiles. Solid triangles, open circles, crosses, and open squares indicate the results of numerical integrations for $\alpha = 1.0, 1.4, 1.6,$ and $1.8,$ respectively. Solid lines represent the best-fits to equation (21) with using equation (24).

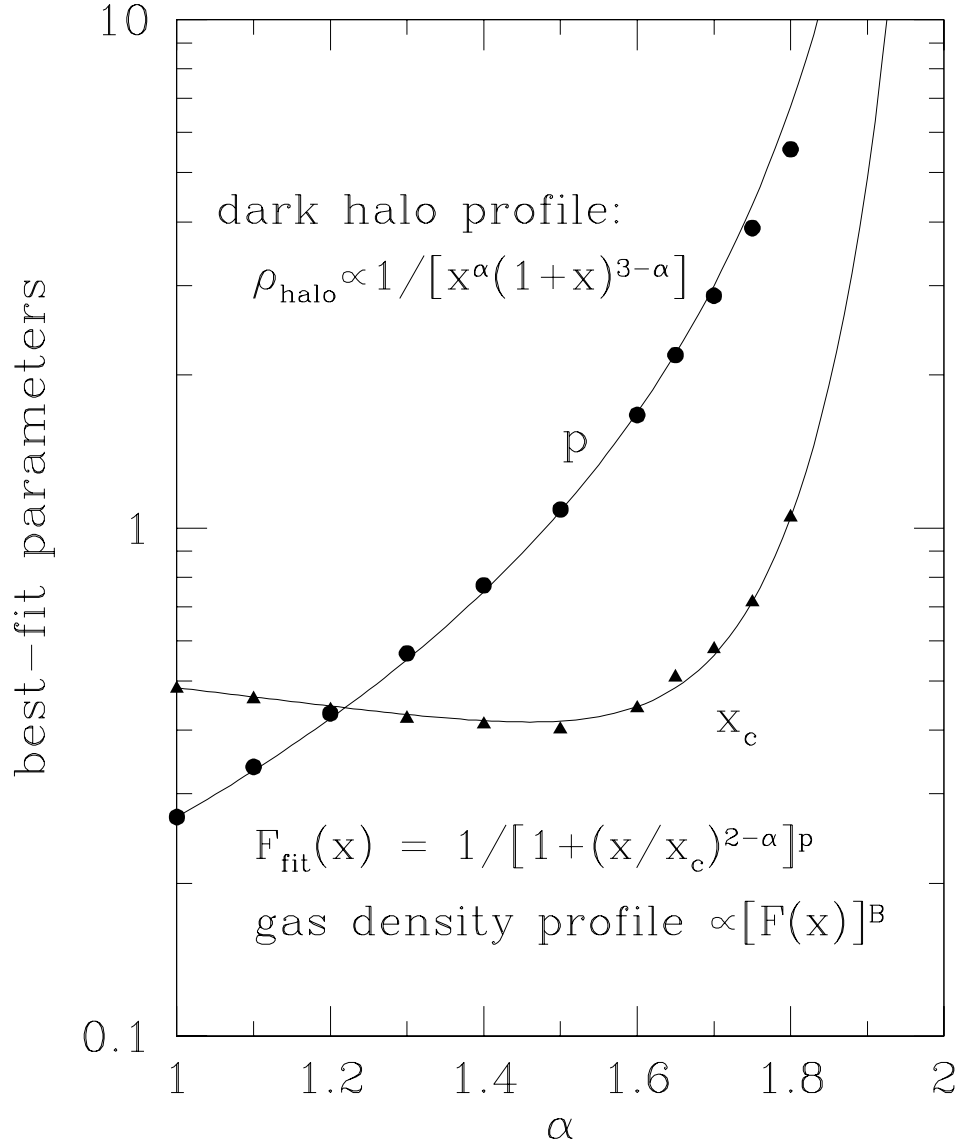


Fig. 2.— The best-fit parameters of x_c and p as a function of α . Solid lines represent the fitting formula (eq.[24]) which is accurate for $1.0 \leq \alpha \leq 1.6$.

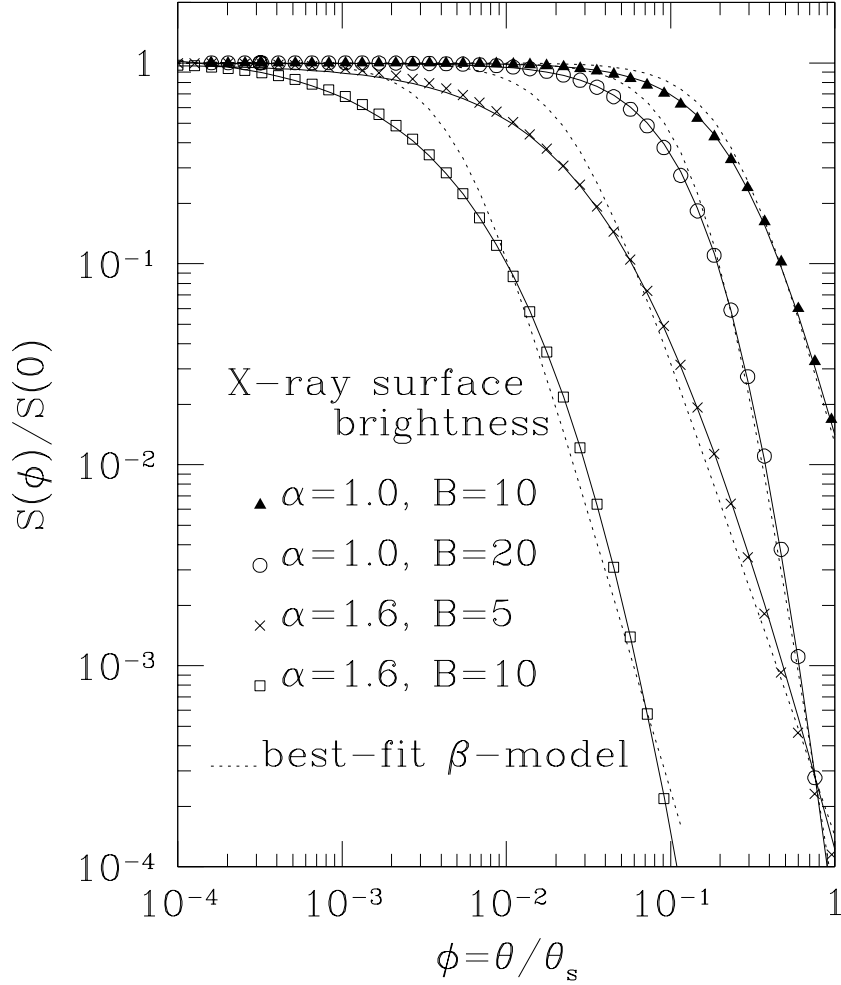


Fig. 3.— X-ray surface brightness profiles predicted from a family of dark matter halo profiles. Filled triangles, open circles, crosses, and open squares indicate the results of numerical integrations for $(\alpha, B) = (1.0, 10.0)$, $(1.0, 20.0)$, $(1.6, 5.0)$, and $(1.6, 10.0)$. Solid lines represent the best-fits to equation (29) with equations (30) to (32), while dotted lines indicate the best-fits to the conventional β -model (eq.[28]).

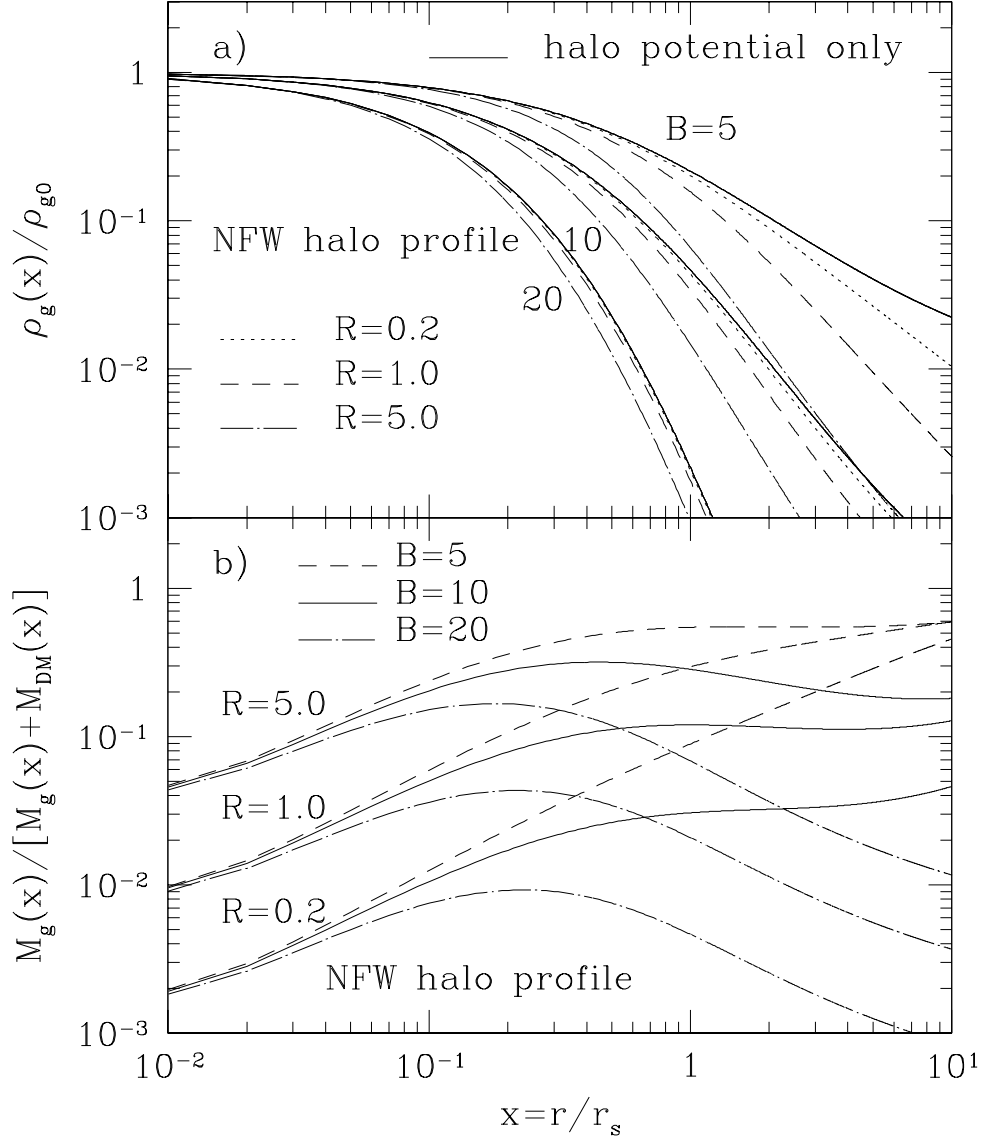


Fig. 4.— Effect of self-gravity of gas density distribution; a) gas density profile normalized in units of the central value; b) gas mass fraction. All models assume $\alpha = 1$ (NFW profile).

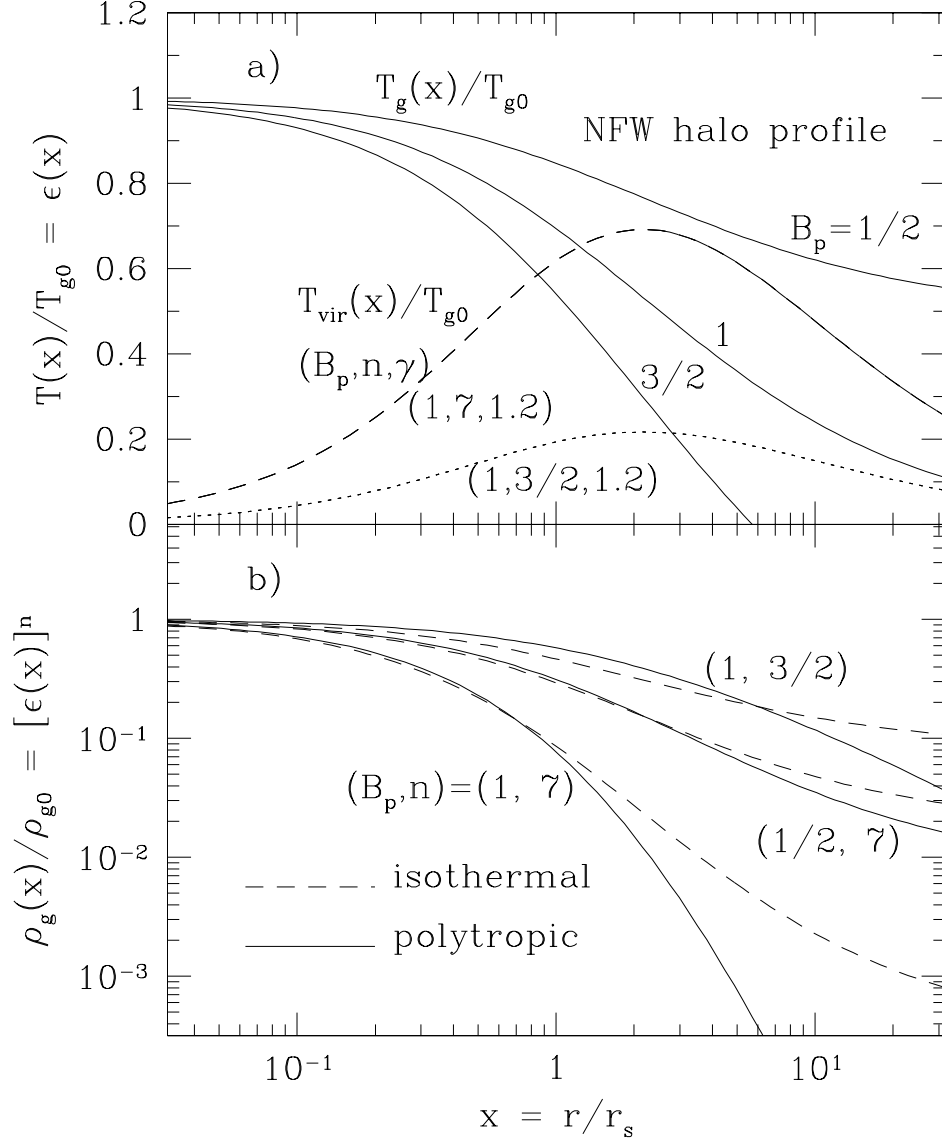


Fig. 5.— Profiles of temperatures and densities for polytropic models embedded in the NFW dark matter halo potential ($\alpha = 1$). a) gas temperatures T_g are plotted in solid lines for $B_p = 0.5, 1.0$ and 1.5 . For reference, the virial temperature T_{vir} is plotted in dashed and dotted lines for $(B_p, n, \gamma) = (1.0, 7, 1.2)$ and $(1.0, 3/2, 1.2)$, respectively. All values are in units of the central gas temperature T_{g0} ; b) gas densities ρ_g for polytropic models (solid lines) and for the corresponding isothermal models (dashed lines) with $B = (n + 1)B_p$ in units of the central value ρ_{g0} .

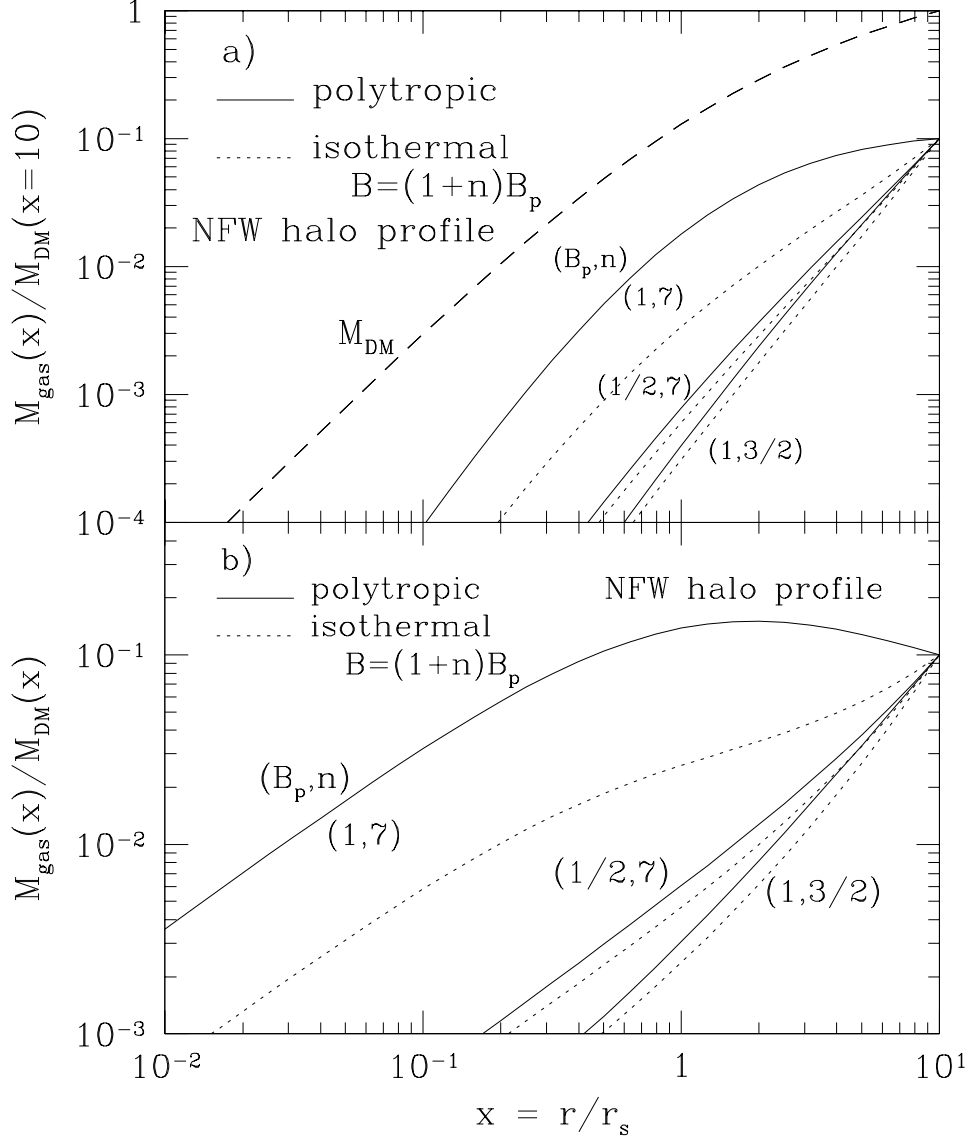


Fig. 6.— Mass profiles for polytropic models embedded in the NFW dark matter halo potential ($\alpha = 1$) with $(B_p, n) = (1.0, 7.0)$, $(0.5, 7.0)$, and $(1.0, 1.5)$. a) gas mass profiles for polytropic models (solid lines) and for the corresponding isothermal models (dotted lines) with $B = (n + 1)B_p$. The gas mass is normalized to be 10 percent of the mass of dark matter halo at $x = 10$. The halo mass profile is plotted in dashed line for reference; b) gas to dark halo mass ratio for polytropic models (solid lines) and for the corresponding isothermal models (dotted lines) with $B = (n + 1)B_p$.

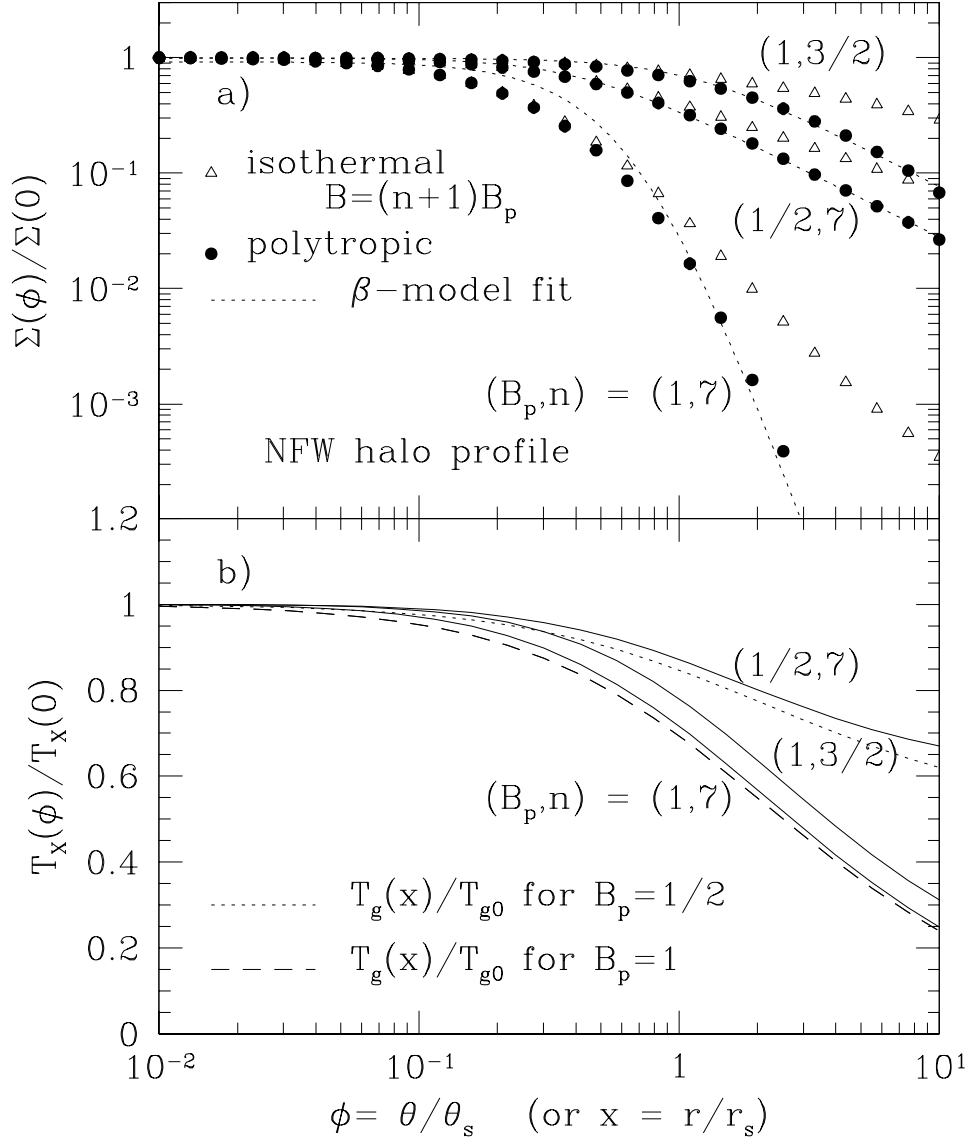


Fig. 7.— X-ray surface brightness and emission-weighted projected temperature profiles for polytropic models embedded in the NFW dark matter halo potential ($\alpha = 1$) with $(B_p, n) = (1.0, 7.0)$, $(0.5, 7.0)$, and $(1.0, 1.5)$. a) bolometric X-ray surface brightness (thermal bremsstrahlung only) profiles for polytropic models (filled circles) and for the corresponding isothermal models (open triangles) with $B = (n+1)B_p$. The dotted lines represent the best-fits to the β model. b) emission-weighted projected temperature profiles for polytropic models (solid lines), gas temperature with $B_p = 1/2$ (dotted line) and $B_p = 1$ (dashed line),